

# Geophysical Research Letters®



## RESEARCH LETTER

10.1029/2021GL093226

## Measurement and Scaling of Lake Surface Skin Temperatures

Miki Hondzo<sup>1,2</sup> , Jiaqi You<sup>1,3</sup>, Jackie Taylor<sup>1,2</sup> , Garret Bartlet<sup>1,2</sup>, and Vaughan R. Voller<sup>1,2</sup> 

### Key Points:

- Natural convection velocity mediate the thickness of diffusive thermal sublayer and the corresponding net heat flux at the interface
- Proposed parameterization of skin-to-bulk temperatures
- Similarity scaling of temperature microprofiles over the diffusive thermal sublayer thickness

### Supporting Information:

Supporting Information may be found in the online version of this article.

### Correspondence to:

M. Hondzo,  
[mhondzo@umn.edu](mailto:mhondzo@umn.edu)

### Citation:

Hondzo, M., You, J., Taylor, J., Bartlet, G., & Voller, V. R. (2022). Measurement and scaling of lake surface skin temperatures. *Geophysical Research Letters*, 49, e2021GL093226. <https://doi.org/10.1029/2021GL093226>

Received 5 MAR 2021  
Accepted 3 MAR 2022

### Author Contributions:

**Formal analysis:** Vaughan R. Voller  
**Investigation:** Jiaqi You, Jackie Taylor, Vaughan R. Voller  
**Validation:** Garret Bartlet  
**Writing – original draft:** Jiaqi You, Jackie Taylor, Vaughan R. Voller  
**Writing – review & editing:** Garret Bartlet

<sup>1</sup>Department of Civil, Environmental, and Geo-Engineering, University of Minnesota, Minneapolis, MN, USA, <sup>2</sup>St. Anthony Falls Laboratory, University of Minnesota, Minneapolis, MN, USA, <sup>3</sup>Institute of Environmental and Ecological Engineering, Guangdong University of Technology, Guangzhou, China

**Abstract** Water temperature microprofiles at the air-water interface of a stratified lake were measured concurrently with moderate wind speeds of 0.8–8.2 ms<sup>-1</sup> above the lake surface. The day-time measurements revealed the cool skin effect of water surface temperatures that triggers the cooling of the lake surface and the occurrence of natural convection. Natural convection velocity scale mediates the thickness of the diffusive thermal sublayer and the corresponding net heat flux at the interface. The diffusive thermal sublayer thickness ranged from 0.7 to 3.6 mm. The temperature microprofiles and proposed parameterization of skin-to-bulk temperatures enable similarity scaling of temperature microprofiles over the diffusive thermal sublayer thickness. The proposed parameterizations allow for the estimation of diffusive thermal sublayer thickness and skin-to-bulk temperature difference in the presence of natural convection. Our results have the potential to facilitate the validation and integration of satellite-derived lake surface temperatures.

**Plain Language Summary** Inland water and ocean surface temperatures are a “global thermometer” of the planet. These water surface temperatures provide an important coupling channel between water and atmosphere environments and mediate the exchange of energy and chemicals between the two. We measured and analyzed temperature profiles in the proximity of air-water interface in a small stratified lake. These measurements revealed a “cool skin” effect—colder water temperatures at the lake surface than those just below it. This cool skin effect triggers the convective cooling of the subsurface water. We propose a model to quantify the cool skin effect in the presence of natural convection. The proposed model can potentially facilitate verification and integration of large-scale measurements of satellite-derived surface water temperatures and may assist the estimation of greenhouse gas transport across lake and ocean surfaces.

## 1. Introduction

Sea surface temperatures (SST) and inland water surface temperatures (IWST) are fundamental physical variables for understanding, monitoring, and predicting fluxes of heat, momentum, and gasses at the air-water interface (AWI). The analyses of SST and IWST data collected by various sensors have contributed to climate research (Donlon et al., 2002; O’Carroll et al., 2019). While several research studies have analyzed SST (Embury et al., 2012; Merchant et al., 2020; Saunders, 1967; Wu, 1971), far less attention has been reported in the investigation of IWST (e.g., Wilson et al., 2013). Inland waters, including lakes and reservoirs, have more heterogeneities and larger wind stress variabilities than ocean waters.

Surface water temperatures are often classified as skin or bulk temperatures, referencing the depth at which they are measured. At the AWI, infrared sensors measure the temperature of the very thin surface or “skin” layer of water. The thickness of the surface skin layer is on the order of micrometers. Over a few centimeters below the surface, water temperatures transitions to a nearly uniform temperature, commonly referred to as bulk temperature. Bulk temperature is consistently warmer than skin temperature by a few tenths of a degree Celsius. This temperature difference is known as the *cool skin effect* or *cool skin*, which implies cooling of the waterside of the AWI and the occurrence of natural convection due to the unstable nature of the associated density profile. The thickness of the cool skin transition layer from the skin temperature to bulk temperature depends on the local heat flux at the AWI. The parameterizations of skin-to-bulk temperature transitions do not include natural convection that potentially affects the water layers in the proximity of the AWI (Bouffard & Wüest, 2019). Understanding the physical processes that control the cool skin effect is important for (a) correlating satellite derived skin temperature data with *in situ* bulk temperature; (b) transforming skin temperature measurements to bulk temperatures, needed to quantify greenhouse (CO<sub>2</sub>, CH<sub>4</sub>, N<sub>2</sub>O) gas transport at the AWI, and (c) determining the water

© 2022. The Authors.

This is an open access article under the terms of the [Creative Commons Attribution-NonCommercial-NoDerivs License](https://creativecommons.org/licenses/by/4.0/), which permits use and distribution in any medium, provided the original work is properly cited, the use is non-commercial and no modifications or adaptations are made.

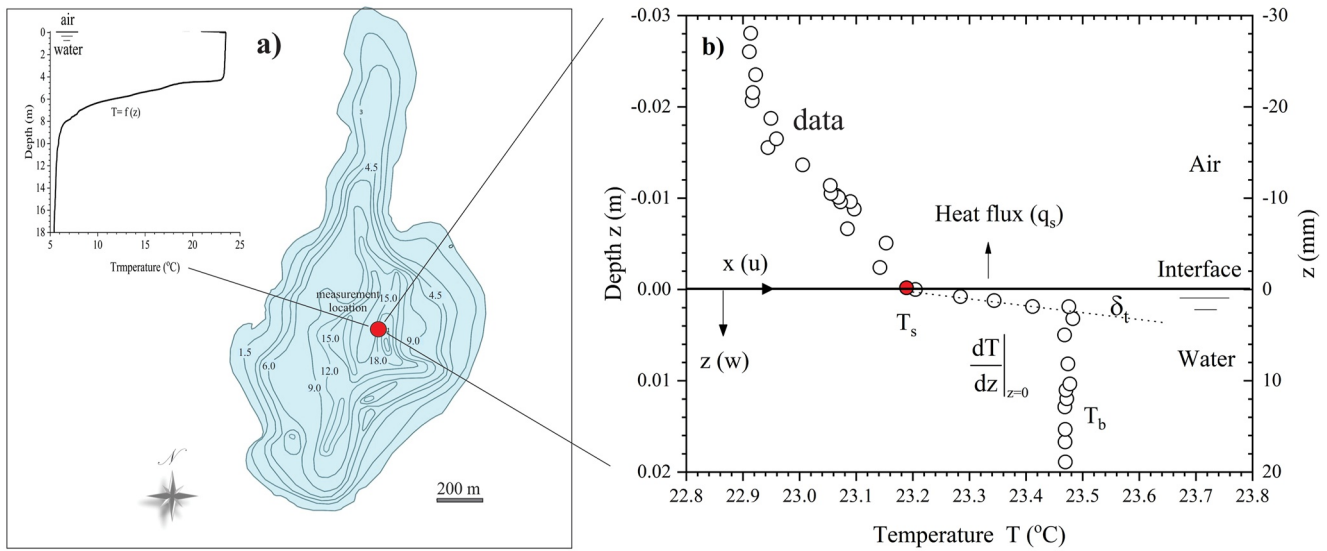


**Figure 1.** Example of a measured water temperature microstructure profile in Ramsey Lake, Wright County, Minnesota, USA. (a) Vertical profile of water temperature over the depth at the measurement location. (b) Measured water temperatures near the air-water interface (AWI), the diffusive thermal sublayer (DTS) thickness ( $\delta_t$ ), schematic of the temperature gradient, dotted line, at the AWI ( $\frac{dT}{dz}|_{z=0}$ ), bulk water temperature ( $T_b$ ) outside of  $\delta_t$ , and  $z$  is the vertical coordinate from the AWI (positive downward) in the water column.

temperature measurement biases of the large number of satellite sensors that contribute to planetary datasets (Merchant et al., 2020).

We analyze *in situ* observations of temperature microstructure profiles and local meteorological conditions at Ramsey Lake, Minnesota, to quantify the cool skin in a small freshwater lake. Following Fourier's law of heat conduction, the local heat flux is estimated from the water temperature gradient and conductivity in the thin layer below the AWI. This thin region is called the diffusive thermal sublayer (DTS). The analysis of DTS thickness and local fluid flow variables provides: (a) parameterization of the DTS, (b) a physical model that quantifies the skin-to-bulk temperature transition, and (c) an estimate of the DTS temperature profile.

## 2. Materials and Methods

### 2.1. Study Site

Ramsey Lake (45°12'27"N, 93°59'43"W) is a residential and recreational lake located in Wright County in Minnesota, USA (Figure 1a). The lake has a surface area of 1.28 km<sup>2</sup> and a maximum depth of 24.4 m with a mean depth of 6.5 m. In summer the lake has a stable thermal stratification and in May and November, of each year, the temperature through the lake depth is approximately uniform.

### 2.2. Temperature and Wind Speed Measurements

A floating research station, designed and built at the St. Anthony Falls Laboratory (University of Minnesota), was deployed and anchored on Ramsey Lake from July to October 2018. The research station's measurement location had a water depth of 18.0 m, enabling temperature profiling through the epilimnion, metalimnion, and hypolimnion (Figure 1a). The research station conducted synchronized monitoring of (a) wind speed and air temperature at 1.5 m above the water surface, and (b) water temperatures at 12 depths from 0.05 m to the bottom of the lake. The meteorological station and the thermistor chain collected data every 6 s and saved averaged data every 5 min. All the data were transferred to the central data logger (Campbell Scientific, CR1000, UT, USA), from which users uploaded the data via wireless telemetry to a server.

A Self-Contained Autonomous Microstructure Profiler (SCAMP, Precision Measurement Engineering, CA, USA) was used to measure and record high resolution profiles of water temperature, conductivity, pressure, and depth in the water column. On deployment, the microprofiler descends from the water surface to the bottom of

the lake, resides at the bottom for typically 5 minutes, and is set in motion from the bottom of the lake to the water surface with an approximate speed range from 0.07 to 0.12 ms<sup>-1</sup> while collecting temperature, conductivity, pressure, and time data at 100 Hz. A fast-response FP07 microthermistor measured the temperatures with an approximate accuracy of 0.001°C and time constant of 7 milliseconds. The resulting spatial resolution of the measurements was around 1.0 mm (100 mm/s × 0.01 s). The data from the fast-response micro-conductivity measurement having similar spatial resolution as the temperature were explored to detect the position of AWI since water has nearly 25 times larger thermal conductivity than air at similar temperatures. At the AWI ( $z = 0$ ), the conductivity profile depicted a significant abrupt step change as the SCAMP transitioned from the water phase to the air phase. The time-interval between successive SCAMP profiles was on average 5 min, and the measurements generally started around 11 a.m. We report a total of 33 independent measurements in Ramsey Lake during the summer of 2018 in July, August, and September. The reported microprofiles consistently depicted higher temperatures on the waterside of AWI than in the air above it.

### 2.3. Temperature Microprofiles and Heat Fluxes at the Air-Water Interface

The waterside heat flux at the AWI can be estimated following Fourier's law of heat conduction (Fourier & Freeman, 1888; Saunders, 1967; Wu, 1971; Wilson et al., 2013):

$$q_s = -k \left. \frac{dT}{dz} \right|_{z=0} \quad (1)$$

where  $q_s$  is the net heat flux out of the water,  $k$  is the conductivity of water,  $T$  is the temperature,  $dT/dz|_{z=0}$  is the local temperature gradient at the AWI (i.e., the cool skin gradient), and  $z$  is the vertical distance below the water surface (Figure 1b). Negative net heat flux implies cooling of the lake surface.

Accurate estimation of  $q_s$  inherently depends on the temperature gradient at the AWI being correctly estimated. The cool skin thickness,  $\delta_t^b$ , has been investigated as an essential component in the calculation of  $q_s$  (Saunders, 1967; Wilson et al., 2013; Wu, 1971) assuming a constant temperature gradient (linear temperature profile) through the cool skin region and thus  $\left. \frac{dT}{dz} \right|_{z=0} \sim \frac{(T_b - T_s)}{\delta_t^b}$  and

$$q_s \approx -\frac{k}{\delta_t^b} (T_b - T_s) \quad (2)$$

where  $T_b$  is the (nearly constant) bulk temperature immediately below the cool skin layer, and  $T_s$  is the water temperature at the AWI (Figure 1b). Cool skin temperature transitions from  $T_s$  to  $T_b$ , where heat conduction is the dominant heat transport process and is defined as the DTS.

A scaling expression for the vertical temperature distribution over  $\delta_t^b$  in the presence of natural convection can be derived by simplifying the steady-state energy equation in the proximity of the AWI. The energy equation reads

$$u \frac{\partial T}{\partial x} + w \frac{\partial T}{\partial z} + \frac{\partial}{\partial z} \left( \frac{q}{\rho c_p} \right) = \frac{\partial}{\partial z} \left( \frac{Q}{\rho c_p} \right) \quad (3)$$

where  $u$  is the velocity in the horizontal  $x$ -direction (Figure 1b),  $w$  is the velocity in the vertical  $z$ -direction,  $\rho$  is the density,  $c_p$  is the specific heat of water, and  $Q$  is the radiation heat flux. Since  $\delta_t^b$  has a length scale on the order of millimeters, it is reasonable to assume an insignificant change of “ $Q$ ” and “ $w$ ” over the  $\delta_t^b$  ( $\partial Q/\partial z$  and  $\partial w/\partial z \sim 0$ ). Furthermore, we presume a small temperature change in the  $x$ -direction (along the lake) in comparison to the change in the vertical direction ( $\partial T/\partial x \ll \partial T/\partial z$ ). Therefore, the energy Equation 3 can be simplified as follows

$$w \frac{dT}{dz} + \frac{1}{\rho c_p} \frac{dq}{dz} = 0 \quad (4)$$

Equation 4 is readily rearranged into the initial value problem in terms of the heat flux  $dq/dT = -w \rho c_p$  with the integration boundaries from  $q_s$  to  $q$  and  $T_s$  to  $T$  which has the solution

$$\frac{q}{q_s} = 1 + \frac{w \rho c_p}{q_s} (T_s - T) = 1 + T^+ \quad (5)$$

where  $q$  is the heat flux and  $T^+ = \rho c_p w (T_s - T)/q_s$  is the dimensionless temperature. The particular case of  $w = 0$ , the absence of natural convection, implies equality between the local heat flux and the heat flux at the AWI ( $q = q_s$ ), which is the heat flux defined in Equation 1. The presence of natural convection, sinking water parcels with positive (downward) vertical velocity ( $w$ ) generated by the cooling at the AWI, is equivalent to the introduction of “blowing” fluid in the diffusive thermal boundary layer, which reduces the thickness of  $\delta_t$ .

### 3. Results and Discussion

#### 3.1. Wind Stress at the Air-Water Interface

The wind speed ranged from 0.8 to 8.39 m s<sup>-1</sup> above the lake surface (Table S1 in Supporting Information S1). The wind-generated surface shear stress leads to downward transport of horizontal momentum through vertical advection and diffusion. The stress or equivalent momentum flux is estimated by  $\tau = \rho_a C_{10} U_{10}^2$  where  $\rho_a$  is the density of air,  $C_{10}$  is the drag coefficient, and  $U_{10}$  is the wind speed at 10 m above the lake surface. Several empirical relationships have been reported for the estimation of  $C_{10}$  from wind data (e.g., Lorke & Wüest, 2003). Generally, at low wind speeds ( $U_{10} < 3$  ms<sup>-1</sup>), the stress is parameterized by an empirical expression proposed by Lorke and Wüest (2003). At more substantial wind speeds ( $U_{10} > 3$  ms<sup>-1</sup>), the functional relationship presented by Charnock (1955) has been used. The estimates of  $C_{10}$  for measured wind speeds are provided in Figure S1 in Supporting Information S1. The maximum value of  $C_{10} = 0.0057$  was estimated at the lowest wind speed ( $U_{10} = 0.80$  ms<sup>-1</sup>), and the minimum of  $C_{10}$  value (0.0009) occurred was at an intermediate range of wind speeds ( $U_{10} = 3.79$  ms<sup>-1</sup>). The overall functional dependence of  $C_{10}$  versus  $U_{10}$  depicted power-law scaling (Figure S1 in Supporting Information S1).

On the waterside of the air-water interface, the surface wind stress induces a turbulent momentum flux, which in concert with the buoyancy flux mixes water layers in proximity to the AWI. The wind induced momentum transfer is characterized by the water friction velocity,  $u_* = \sqrt{\tau \rho^{-1}}$ , and actively mixes water layers in the proximity of the AWI but below  $\delta_t^b$ . The estimated average value of  $u_*$  was 0.0057 ms<sup>-1</sup> (Table S1 in Supporting Information S1). We define a horizontal layer of the water column below  $\delta_t^b$  that is nearly uniform in temperature ( $T_b$ ) as the actively mixed layer with thickness “ $h$ ”. The criterion used to estimate  $h$  was the location of the first temperature below  $\delta_t^b$  that was cooler by 0.02°C than  $T_b$  (Tedford et al., 2014). The actively mixed layer thickness varied from 0.1 to 1.37 m with an average value of 0.47 m (Table S1 in Supporting Information S1).

#### 3.2. Temperature Profiles at the Air-Water Interface

Over the lake depth at the measuring location, water temperatures depicted stable stratification (Figure 1a) with the exception of the cool skin surface layer which exhibited negative buoyancy flux (Figure 1b). This negative buoyancy flux was due to cooling at the AWI. The average water temperature difference ( $\Delta T = T_b - T_s$ ) across  $\delta_t^b$  was 0.27°C with a maximum value of 0.82°C and a minimum of 0.02°C. The net heat loss at the lake surface is proportional to  $\Delta T$  and inversely related to  $\delta_t^b$ . We estimated the net heat flux,  $q_s$ , from the temperature gradient,  $dT/dz|_{z=0}$ , through  $\delta_t^b$  (Equation 2). The heat flux ranged from 5.1 to 358.0 Wm<sup>-2</sup> with an average value of 98.0 Wm<sup>-2</sup>. At the AWI, the buoyancy flux,  $B$ , was driven by  $q_s$ , which is estimated from  $B = g/\rho \alpha/c_p q_s$  (Table S1 in Supporting Information S1). We assume negligible contribution of the fluxes of salinity and suspended particles in the estimation of  $B$ . The flux was negative and varied from  $2.88 \cdot 10^{-9}$  to  $2.0 \cdot 10^{-7}$  m<sup>2</sup>s<sup>-3</sup> (Table S1 in Supporting Information S1). This flux caused mixing in and thickening of the actively mixed layer. The convective velocity scale in the vertical direction can be estimated by  $w_* = (|B|h)^{1/3}$  (Deadroff, 1970). The thickness of the actively mixed layer can be calculated from the temperature microprofiles data, which integrates all the sources and sinks of heat in the water column. The opposing effects of heating by shortwave radiation and cooling by natural convection are combined in the actively mixed layer. The average  $w_* = 0.0025$  ms<sup>-1</sup> was approximately two times smaller than the corresponding velocity scale  $u_*$  (Table S1 in Supporting Information S1).

The average  $\delta_t^b$  was 2.0 mm and ranged from 0.71 to 3.59 mm (Table S1 in Supporting Information S1). The average ratio  $\frac{\delta_t^b}{h}$  was 0.4%. Several attempts were explored to establish a statistically significant scaling relationship between  $\delta_t^b$  and the available data and associated derived variables. The customarily used shear velocity,  $u_*$ , did not reveal any significant statistical dependence with  $\delta_t^b$ .  $\delta_t^b$  versus  $w_*$  showed a negative and statistically significant ( $r^2 = 0.69$ ) functional dependence (Figure 2). It is theorized that at the macroscopic scale, the negative

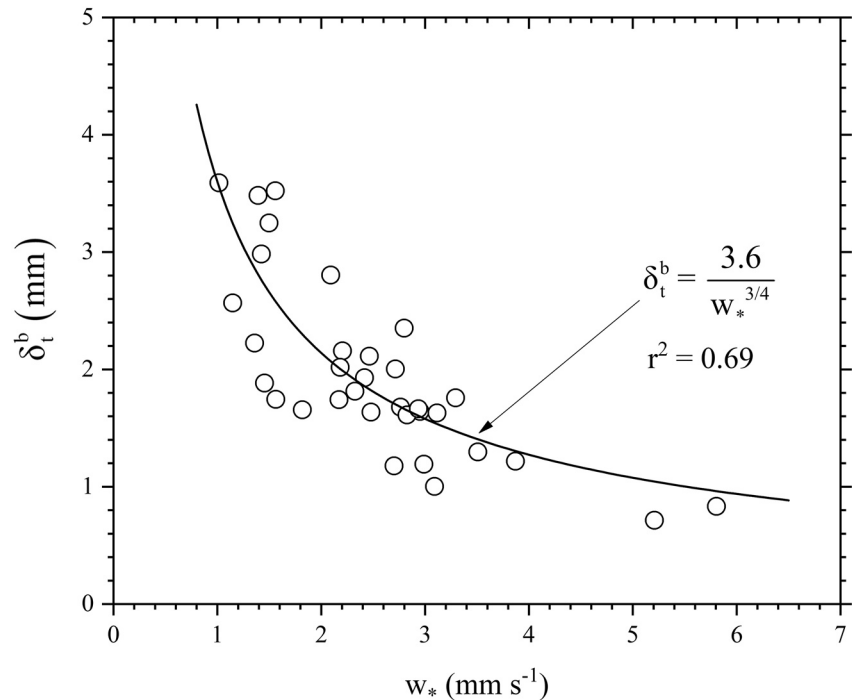


**Figure 2.** Dependence of diffusive thermal sublayer thickness ( $\delta_t^b$ ) on the convective velocity scale ( $w_*$ ).

heat flux at the AWI triggered the convection of the negatively buoyant fluid having a  $w_*$  velocity scale, in turn increasing  $h$ . At the microscopic scale,  $w_*$  and associated well-documented mushroom-type currents (Bouffard & Wüest, 2019) provided a flux of water from the cool skin to actively mixed layers causing the thinning of  $\delta_t^b$ .

Turbulent wall-bounded flows have been used to model the skin-to-bulk temperature regime or skin effect ( $\Delta T = T_b - T_s$ ) over the ocean. The DTS has been approximated as the fraction of the viscous-sublayer thickness given by  $\delta_v = \lambda \nu / u_*$  where  $\lambda$  is an empirical constant (Saunders, 1967), and  $\nu$  is the kinematic viscosity. Several values of  $\lambda$  have been reported, ranging from 2 to 8 for wind speeds from 1 to 11  $\text{ms}^{-1}$  (Wilson et al., 2013). In our study, we did not observe significant statistical dependence of the form  $\Delta T \sim q_s / u_*$  nor  $\Delta T \sim q_s / w_*$ . The most substantial statistical support found ( $r^2 = 0.58$ ) was for the scaling relationship of  $\Delta T \sim u_* / w_*$  (Figure 3). Soloviev and Schlüssel (1996) and Soloviev and Lukas (2014) proposed a scaling relationship  $\Delta T \sim (P_r R_{i0} K_c)$ , where  $P_r$  is the Prandtl number,  $R_{i0}$  is the surface Richardson number, and  $K_c$  is the Keulegan number. If the role of surface waves is neglected ( $K_c = 0$ ), the scaling relationship can be simplified (Figure S2 in Supporting Information S1). This simplified scaling relationship depicted a good agreement with our data ( $r^2 = 0.68$ ). Furthermore, the scaling relationship presented in Figure S2 in Supporting Information S1 can be expanded into a Taylor series and arranged in a form  $\Delta T \sim f(u_* / w_*)$  which is in general concert with the scaling relationship in Figure 3, only simplified.

### 3.3. Scaling Temperature Profiles

The temperature microprofiles and Equation 5 provided the background for verifying the scaling of temperature distribution over the DTS thickness. An underlying approximation that is embedded in Equation 5 is the order of magnitude of  $\partial T / \partial x$  versus  $\partial T / \partial z$  in the proximity of AWI. The SCAMP measurements were conducted from the fixed platform at the measuring location (Figure 1a) which enabled the estimation of spatial distance at water surface breaking locations. The average  $x$ -direction distance between two SCAMP locations at the AWI was about 2.5 m. The corresponding average temperature difference,  $T_s$ , was about  $0.18^\circ\text{C}$  which provided an estimate of  $\partial T / \partial x|_{z=0} \approx -0.18 \text{ Cm}^{-1}$ . The  $\partial T / \partial x|_{z=0}$  was significantly smaller than the average  $\frac{\partial T}{\partial z}|_{z=0} \approx 164 \text{ Cm}^{-1}$  (Table S1 in Supporting Information S1). Also, we assumed an insignificant change of  $Q$  over the DTS thickness. An average summer light attenuation coefficient in the lake was  $k_d \sim 1.5 \text{ m}^{-1}$  with an average noon incident shortwave

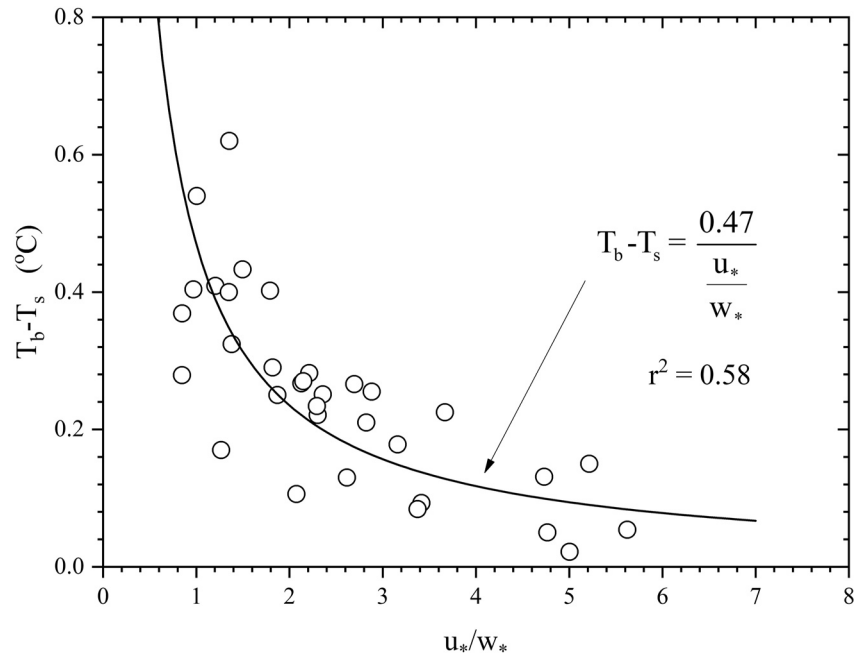


**Figure 3.** The water temperature difference between surface temperature ( $T_s$ ) and bulk temperature ( $T_b$ ) over the diffusive thermal sublayer thickness ( $\delta_t^b$ ) as a function of the ratio of shear velocity scale ( $u_*$ ) at the air-water interface and convective velocity scale ( $w_*$ ).

radiation  $Q_o \sim 100 \mu\text{Em}^{-2}\text{s}^{-1}$ . The corresponding water temperature difference due to the radiation absorption over the DTS was significantly less than the fast-response FP07 microthermistor accuracy ( $\frac{\Delta Q_{\delta_t^b}}{\rho c_p} \ll 0.001^\circ\text{C}$ ).

The proposed scaling of temperature distribution over the DTS thickness as a function of the non-dimensional vertical distance ( $z^+ = u_* z / \nu$ ) from the AWI is depicted in Figure 4. The data indicate a statistically significant ( $r^2 = 0.76$ ) functional dependence

$$\frac{\rho c_p w_* (T_s - T)}{q_s} = 2.1 \frac{u_* z}{\nu} \text{ for } \delta_t^b \geq z \geq 0 \quad (6)$$

All the reported temperature profiles depicted the cooling of AWI and, therefore,  $T > T_s$  and  $q_s < 0$ . The proposed scaling suggests that both the wind with the corresponding turbulent momentum flux ( $u_*$ ) and natural convection with a velocity scale ( $w_*$ ) for a given heat flux ( $q_s$ ) at the AWI determine the temperature distribution over the DTS thickness. A parameterization of night-time skin effect ( $T_s - T_b$ ) was proposed in terms of wind speed by (Donlon, 2002; Embury et al., 2012) and was suggested to be applicable during the day-time at high wind speeds ( $> 7 \text{ ms}^{-1}$ ) (Minnett et al., 2011).

#### 4. Conclusions

We measured lake temperature microprofiles and meteorological conditions in and on a small stratified lake during the summer of 2018. The wind speed above the lake surface ranged from  $0.8$  to  $8.4 \text{ ms}^{-1}$ . In the immediate proximity of the water surface the temperature profile depicted a thin cool skin surface layer with bulk temperatures below it warmer on average by  $0.25^\circ\text{C}$  than the temperatures at the air-water interface. The temperature difference induced cooling at the lake surface with an average heat flux of  $100 \text{ Wm}^{-2}$ . The diffusive thermal sublayer (DTS) measured from the temperature profiles had a thickness from  $0.7$  to  $3.6 \text{ mm}$ . The thickness of the DTS was mediated by the natural convection velocity scale and not by the shear velocity scale that is used in wall-bounded turbulent flows. We propose a power-law function that includes the ratio of natural convection and shear velocity scales to quantify the temperature difference between skin temperature and bulk temperature. The existing parameterizations do not include natural convection that affects the near-surface thermal layers in the proximity of the air-water interface (Bouffard & Wüest, 2019). Our data and simplified energy equation suggest

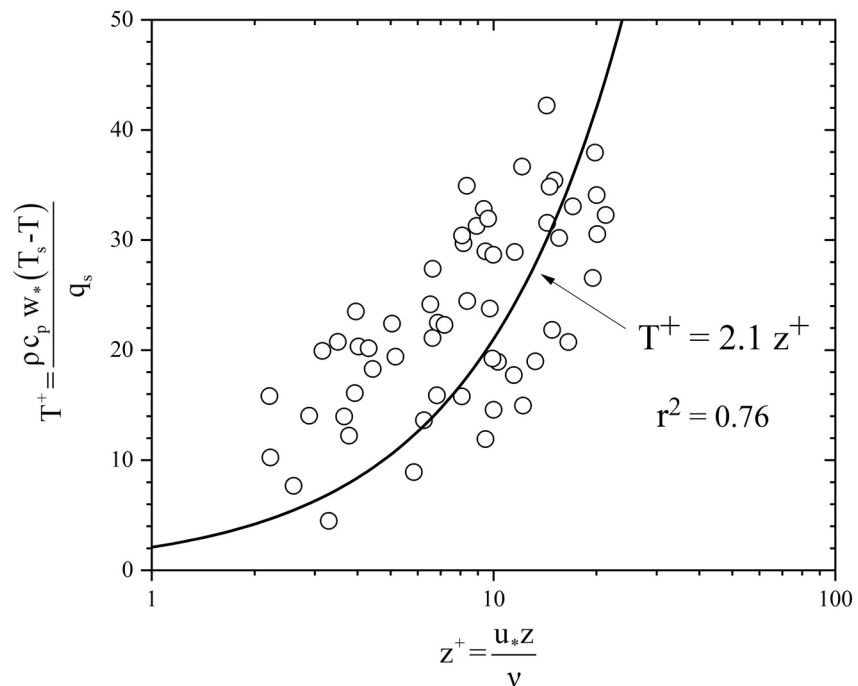


**Figure 4.** Dimensionless water temperature microprofiles ( $T^+$ ) versus downward distance ( $z^+$ ) from the air-water interface. The proposed scaling relationship ( $T^+ = 2.1 z^+$ ) applies over the diffusive thermal sublayer (DTS) thickness.

a scaling relationship for the temperature distribution over the DTS thickness. This scaling relationship includes natural convection velocity and shear stress scales and not simply a wind speed scale as proposed for the nighttime skin effect (Donlon, 2002; Embury et al., 2012) and the day-time skin effect (Minnett et al., 2011) of ocean water surfaces.

The results of our work can contribute to the validation of satellite-derived surface skin temperature measurements. Inland waters play significant roles in the exchange of greenhouse gasses between the Earth's surface and the atmosphere (DelSontro et al., 2018). Accurate quantification of  $\text{CO}_2$ ,  $\text{CH}_4$ , and  $\text{N}_2\text{O}$  fluxes are contingent upon a rigorous estimation of gas transfer velocities and associated diffusive sublayer, where molecular diffusion dominates the transport of gas across the air-water interface, in the presence of natural convection.

## Data Availability Statement

The data used in this study are publicly available in the University of Minnesota Data Repository, University Digital Conservancy, and has the following persistent identifier: <https://hdl.handle.net/11299/226604>.

## Acknowledgments

We conducted this work during the Covid 19 lockdown in the state of MN, USA. During the summer months, a partial support for V. Voller and M. Hondzo was provided by the James L. Record professorship, Department of Civil, Environmental, and Geo- Engineering, University of Minnesota. We are thankful to Dr. Christopher Ellis for providing critical comments and suggestions for the first draft of the manuscript. Dr. Michael Head, Precision Measurement Engineering (PME), Vista California, provided useful comments regarding technical specifications and limitations of the PME temperature and micro-conductivity sensors.

## References

- Bouffard, D., & Wüest, A. (2019). Convection in lakes. *Annual Review of Fluid Mechanics*, 51, 189–215. <https://doi.org/10.1146/annurev-fluid-010518-040506>
- Charnock, H. (1955). Wind stress on a water surface. *Quarterly Journal of the Royal Meteorological Society*, 81, 639–640. <https://doi.org/10.1002/qj.49708135027>
- Deardorff, J. W. (1970). Convective velocity and temperature scales for the unstable planetary boundary layer and for Rayleigh convection. *Journal of the Atmospheric Sciences*, 27(8), 1211–1213. [https://doi.org/10.1175/1520-0469\(1970\)027<1211:cvatsf>2.0.co;2](https://doi.org/10.1175/1520-0469(1970)027<1211:cvatsf>2.0.co;2)
- DelSontro, T., Beaulieu, J., & Downing, J. (2018). Greenhouse gas emissions from lakes and impoundments: Upscaling in the face of global change. *Limnology and Oceanography Letters*, 3, 64–75. <https://doi.org/10.1002/lol2.10073>
- Donlon, C. J., Minnett, P. J., Gentmann, C., Nightingale, T. J., Barton, I. J., Ward, B., & Murray, M. J. (2002). Toward improved variation of satellite sea surface skin temperature measurements for climate research. *Journal of Climate*, 15(4), 353–369. [https://doi.org/10.1175/1520-0442\(2002\)015<0353:tivoss>2.0.co;2](https://doi.org/10.1175/1520-0442(2002)015<0353:tivoss>2.0.co;2)
- Embury, O., Merchant, C. J., & Corlett, G. K. (2012). A reprocessing for climate of sea surface temperatures from the along-track scanning radiometers: Initial validation, accounting for skin and diurnal variability effects. *Remote Sensing of Environment*, 116, 62–78. <https://doi.org/10.1016/j.rse.2011.02.028>

- Fourier, J., & Freeman, A. (1888). *The analytical theory of heat (by J. Fourier and translated, with notes, by A. Freeman)* (p. 466). G.E. Stechert & Co.
- Merchant, C. J., Block, T., Embury, O., Mitaz, J. P. D., & Mollard, J. D. P. (2020). Homogenization of space-borne infra-red sensors measuring sea surface temperature. *Remote Sensing*, *12*(61048), 1–15. <https://doi.org/10.3390/rs12061048>
- Minnett, P. J., Smith, M., & Ward, B. (2011). Measurements of the oceanic thermal skin effect. *Deep Sea Research II*, *51*, 861–868. <https://doi.org/10.1016/j.dsr2.2010.10.024>
- O’Carroll, A. G., Armstrong, E. A., Beggs, H. M., Bouali, M., Casey, C. S., Corlett, G. K., et al. (2019). Observational needs of sea surface temperature. *Frontiers in Marine Science*, *6*, 1–27.
- Saunders, P. M. (1967). Temperature at ocean-air interface. *Journal of the Atmospheric Sciences*, *24*(3), 269–273. [https://doi.org/10.1175/1520-0469\(1967\)024<0269:ttatoa>2.0.co;2](https://doi.org/10.1175/1520-0469(1967)024<0269:ttatoa>2.0.co;2)
- Soloviev, A. V., & Lukas, R. (2014). *The near-surface layer of the ocean: structure, dynamics and applications* (Vol. 48, p. 548). Springer Science and Business Media.
- Soloviev, A. V., & Schlüssel, P. (1996). Evolution of cool skin and direct air-sea gas transfer coefficient during daytime. *Boundary-Layer Meteorology*, *77*(1), 45–68. <https://doi.org/10.1007/bf00121858>
- Tedford, E. W., MacIntyre, S., Miller, S. D., & Czikowsky, M. J. (2014). Similarity scaling of turbulence in a temperate lake during fall cooling. *Journal of Geophysical Research: Oceans*, *119*(8), 4689–4713. <https://doi.org/10.1002/2014jc010135>
- Wilson, R. C., Hook, S. J., Schneider, P., & Schladow, G. S. (2013). Skin and bulk temperature difference at lake Tahoe: A case study on lake skin effect. *Journal of Geophysical Research: Atmospheres*, *118*(10332–10), 346. <https://doi.org/10.1002/jgrd.50786>
- Wu, J. (1971). An estimation of Oceanic thermal-sublayer thickness. *Journal of Physical Oceanography*, *1*, 284–286. [https://doi.org/10.1175/1520-0485\(1971\)001<0284:aeoots>2.0.co;2](https://doi.org/10.1175/1520-0485(1971)001<0284:aeoots>2.0.co;2)
- Wüest, A., & Lorke, A. (2003). Small-scale hydrodynamics in lakes. *Annual Review of Fluid Mechanics*, *35*, 373–412.